Integrated Physics Analysis of Plasma Start-up Scenario of Helical Reactor FFHR-d1

T. Goto, J. Miyazawa, R. Sakamoto, R. Seki, C. Suzuki, M. Yokoyama, S. Satake, A. Sagara, the FFHR Design Group

National Institute for Fusion Science (NIFS), Toki, Gifu, 502-5292 Japan

E-mail: goto.takuya@LHD.nifs.ac.jp

Abstract

1D physics analysis of the plasma start-up scenario of the Large Helical Device (LHD)-type helical reactor FFHR-d1 was conducted. The time evolution of the plasma profile is calculated using a simple model based on the LHD experimental observations. A detailed assessment of the MHD equilibrium and neo-classical energy loss was conducted using the integrated transport analysis code TASK3D. The robust controllability of the fusion power was confirmed by feedback control of the pellet fuelling and a simple staged variation of the external heating power with a small number of simple diagnostics (line-averaged electron density, edge electron density and fusion power). A baseline operation control scenario (plasma start-up and steady-state sustainment) of the FFHR-d1 reactor for both self-ignition and sub-ignition operation modes was demonstrated.

Keywords: heliotron, plasma start-up scenario, reactor design, MHD equilibrium, neoclassical transport

1. Introduction

In anticipation of the construction of a demonstration fusion power plant (DEMO) after ITER, showing the capability of steady-state operation is of great importance. In this respect, helical systems with net-current free plasma have an advantage because there are no disruptive events and no need for a plasma current drive. In particular, the Large Helical Device (LHD) [1], a heliotron-type system with two continuous helical coils, has demonstrated several remarkable achievements including high-beta discharges with a volume-averaged beta value of $<\beta>$ = 5.1%. Based on these achievements, conceptual design of a heliotron-type fusion reactor and related engineering R&Ds have been continuously conducted under the Fusion Engineering Research Project at National Institute for Fusion Science [2].

Recently, conceptual design of the LHD-type helical reactor FFHR-d1 [2] has made great progress. The direct profile extrapolation (DPE) method [3] improves the predictability of the core plasma performance. Based on the core plasma design, primary design parameters at the point of steady-state operation (the major radius of the helical coil winding centre R_c = 15.6 m, the magnetic field strength at the helical coil winding centre B_c ~ 5 T and the fusion power P_{fus} ~ 3 GW) were set using the systems code HELIOSCOPE [4]. Detailed physics assessment of the core plasma at this steady-state operation point was conducted and the core plasma design consistent with MHD equilibrium, neoclassical transport and alpha particle confinement can be realized via the suppression of the Shafranov shift by selecting a high aspect ratio configuration and applying an adequate vertical magnetic field [5]. In contrast, the plasma start-up scenario toward this steady-state operation point should also be considered because a consistent system design can be implemented only with a clearly-defined operation scenario. In past studies, plasma operation control scenarios for LHD-type helical reactors were examined using a 0D model and feedback control of the fusion power by manipulating the fuelling rate was proposed [6]. This direct control of the fusion power is favourable, because it enables control of the plasma using only ex-vessel neutron diagnostics. However, 0D analysis cannot consider changes in the plasma profile. To examine the effect of the change in the plasma profile on the plasma controllability, a 1D calculation code was developed and control of the plasma by pellet

fuelling has been examined using this code in a previous study [7, 8]. However, consistency with MHD equilibrium and neo-classical transport has not yet been fully examined.

This study discusses the results of integrated physics analyses of the plasma start-up scenario of the FFHR-d1 reactor. A review of the developed integrated 1D analysis code is given in Section 2. Discussion of the control method is presented in Section 3. The results of the calculations for both self-ignition and sub-ignition operational conditions are shown in Section 4. Finally, results are summarised in Section 5.

2. Calculation method

2.1. 1D Calculation model

In general, calculating the time evolution of the plasma radial profile is done by solving the diffusion equation of plasma density and temperature with particle and thermal diffusion coefficients obtained from experimental data or numerical simulations. However, such a detailed numerical simulation requires long computational time and fully predictable models have not yet been established. Therefore, in this study, a simplified model developed for the analysis of the pellet fuelling requirements [7] was used.

In this model, the time evolution of the electron density n_e is calculated by solving a 1D diffusion equation with cylindrical geometry as follows:

$$\frac{\partial n_e}{\partial t} = \frac{1}{r}\frac{\partial}{\partial r}\left\{ r\left(D\frac{\partial n_e}{\partial r} - n_e V \right)\right\} + S \,. \quad (1)$$

On the basis of the experimental observation of typical pellet-fuelled discharges of LHD, no advection flow ($V = 0$) and the following spatially constant diffusion coefficient are assumed:

$$D(r) = D \propto \left(P_{\mathrm{abs}}/\overline{n}_e\right)^{0.6} B_{\mathrm{ax}}^{-0.8}, \quad (2)$$

where P_{abs}, $\overline{n}_e$ and B_{ax} are the total absorbed power, the line-averaged electron density and the magnetic field strength at the magnetic axis, respectively. The time evolution of electron temperature is calculated from that of electron pressure. In the LHD experiment, gyro-Bohm-type dependence is recognised in not only global confinement but also the relation between the local electron density and the electron pressure ($p_e(r) \propto n_e(r)^{0.6}$) [3]. Based on this gyro-Bohm-type parameter dependence, the time evolution of the electron pressure is estimated as follows:

$$\frac{\partial p_e(r)}{\partial t} = \frac{1}{\tau_E}\left(\gamma_{\mathrm{DPE}*}\hat{p}_e(r) P_{\mathrm{abs}}^{0.4} B^{0.8} n_e(r)^{0.6} - p_e(r)\right), \quad (3)$$

where τ_E and $\gamma_{\mathrm{DPE}*}$ are the energy confinement timeand the confinement improvement factor estimated from the heating profile [9], respectively. $\hat{p}_e(r)$ is the gyro-Bohm normalised electron pressure of the reference LHD experimental data:

$$\hat{p}_e(r) = \frac{p_{e,\mathrm{exp}}(r)}{P_{\mathrm{abs,exp}}^{0.4} B_{\mathrm{exp}}^{0.8} n_{e,\mathrm{exp}}(r)^{0.6}} \,. \quad (4)$$

In the calculation, this gyro-Bohm normalised electron pressure is approximated by the fitting function of the normalised minor radius ρ. To consider the profiles with internal transport barrier (ITB), the fitting function was modified from a single zero-order Bessel function given in Ref. [5] to a sum of the Bessel and Gauss functions as follows:

$$\hat{p}_e(\rho) = \alpha_0 J_0\left(\frac{2.4\rho}{\alpha_1}\right) + \alpha_2 \exp\left(-\frac{\rho^2}{2\alpha_3^2}\right). \quad (5)$$

The electron density is fitted by the following formula:

$$n_e(\rho) = \frac{n_{e0}}{1-\alpha_4}\left\{\left[1-\left(\frac{\rho}{\alpha_1}\right)^{\alpha_5}\right]-\alpha_4\left[1-\left(\frac{\rho}{\alpha_1}\right)^{2}\right]\right\}. \qquad (6)$$

We also assume plasma charge neutrality and temperature equality of the electrons and ions.

Assuming fuelling by pellet injection, the final (density source) term of Eq. (1) is given as the radial profile of the pellet ablation, which is estimated by the neutral gas shielding (NGS) model [10]. Adiabatic changes in the electron density and temperature are assumed at the timing of the pellet ablation.

Because the estimation method of the radial profile of the electron pressure mentioned above is a type of 'abductive' approach, it can exclude ambiguity and arbitrariness in prediction models. In contrast, consistency with the results of detailed physics analyses, including MHD equilibrium and neo-classical transport, should be examined. Thus, this 1D code is coupled with several modules of the integrated transport analysis suite TASK3D [11]. The geometric shape of the flux surfaces is calculated by VMEC [12] with the pressure profile of each time slice. The energy flux by neo-classical transport at each flux surface is evaluated using GSRAKE [13] with the radial profiles of the plasma density and temperature, and compared with the total energy generated inside the flux surface. A schematic of the calculations using the integrated 1D analysis code is shown in Fig. 1.

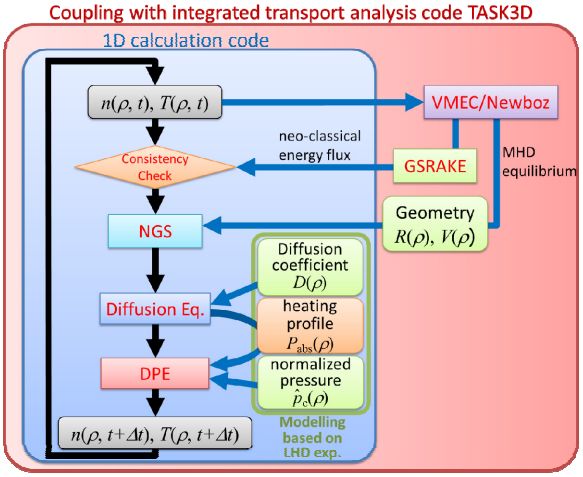

Figure 1. Schematic of the calculations using the integrated 1D analysis code.

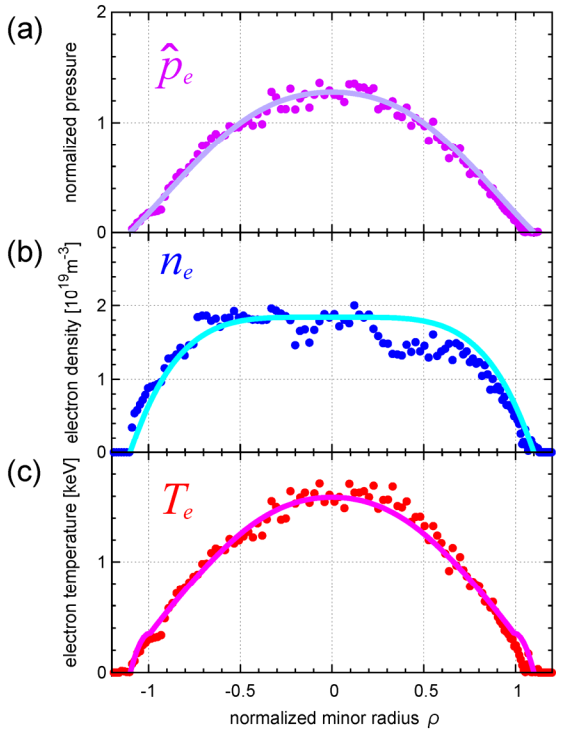

Figure 2. Radial profile of (a) the gyro-Bohm normalised electron pressure used in the calculations and (b) the electron density and (c) the electron temperature of the LHD experimental data used as the reference (#115787, t = 3.90 s, $R_{ax,vac}$ = 3.55 m, B_{ax} = 1.0 T, γ_c = 1.20). Closed circles are data measured by Thomson scattering and the solid lines are the fitting results using Eqs. (5) and (6).

2.2. Prerequisites of the calculation

In this study, the radial profile of the gyro-Bohm normalised electron pressure obtained in the LHD experiment was used as the reference profile (Fig. 2(a)). This profile was obtained with the magnetic configuration of the inward-shifted magnetic axis position (a ratio between the magnetic axis position R_{ax} and the major radius of helical coil winding centre R_c of 3.55/3.9) and high plasma aspect ratio with helical pitch parameter γ_c = 1.2 (where $\gamma_c = ma_c/(lR_c)$ and m, a_c and l are the toroidal pitch number, helical coil minor radius and the number of helical coils, respectively) was used. These profiles correspond to that of 'FIS-HA-MPD' presented in Ref. [5], which can achieve high-beta (peak value of ~8%) equilibrium with the shape of the flux surfaces similar to that in vacuum equilibrium and neo-classical heat loss of roughly half of the absorbed heating power

by applying a vertical magnetic field. In the previous study [8], an increase in the magnetic field strength was proposed to keep the minimum achievable fusion power ~3 GW. Therefore, in this study, the reference radial profile was extrapolated to the FFHR-d1 (R_c = 15.6 m) with B_c = 5.6 T.

In the calculation of the diffusion equation (Eq. (1)), a Dirichlet boundary condition is assumed; the electron density at the plasma boundary (corresponding to ρ = 1.1 in this case) is fixed to zero. It was found that VMEC calculations with a free-boundary condition give an overestimation in the evaluation of the shift of magnetic axis and peripheral magnetic surfaces especially in high-beta conditions [14]. In contrast, calculations using HINT code with experimentally obtained pressure profiles are good agreement with experimental data [15]. As mentioned above, the existence of the equilibrium with the same boundary shape as that in vacuum was confirmed using HINT2 code up to the peak beta value of ~8% in a previous study [16]. Thus, in the calculation of MHD equilibrium by VMEC, the shape of the last closed flux surface (LCFS) was fixed as that in vacuum equilibrium.. To determine the essential parameters needed to establish a basic control algorithm as the first step, ideal conditions of the core plasma (complete absorption of the alpha and external heating power, no impurity accumulation) were assumed for simplicity. In this study, the effect of the deposition profile of the heating power is not considered except for the evaluation of the confinement improvement factor γ_{DPE*} in Eq. (3). In the evaluation of γ_{DPE*}, the radial profile of the alpha heating power deposition is assumed to be identical with that of the alpha power generation. For the external heating, ideal core heating (complete power deposition in the region of $\rho < 0.2$) was assumed. In the calculation of neo-classical transport using GSRAKE, pure deuterium plasma was assumed due to limitations in the code. The ambipolar radial electric field was self-consistently solved in the calculation so that the equality of the particle flux of ions and electrons was satisfied on every flux surface.

For the pellet fuelling, the injection of a fixed size pellet (containing 2×10^{22} particles) is assumed with an injection velocity of 1.5 km/s, which can be implemented without special technological development. The minimum injection interval was set as 5 ms considering the time resolution of the density measurement.

3. Control algorithms

3.1. Consideration of control algorithm of external heating power

In our previous study without equilibrium calculations, it was shown that direct feedback control of the fusion power is difficult due to the time delay in the response of the fusion power corresponding to the density diffusion time constant. Feedback control of the line-averaged electron density was proposed [8] instead of the fusion power, because it promptly responds after the pellet injection and there are several types of well-established diagnostics. In this study, the same feedback control method was adopted. Because pellet injection with a fixed size and a finite interval is assumed, as described above, the actual control results in simple on–off control.

Pre-programmed control of the external heating power was adopted in the previous study [8] and an adequate control method needed to be established. Therefore, in this study, we examined the effect of the external heating power during the plasma start-up (i.e., phase where density increases). If the heating power is insufficient, the edge electron density exceeds the Sudo density limit, resulting in the termination of the plasma [17]. Because the electron density limit is proportional to the square root of the total absorbed power ($n_{e,\mathrm{Sudo}} \propto \sqrt{P_{\mathrm{abs}}}$), an increase in the external heating power directly increases the margin for the edge electron density. An increase in the external heating power also leads to an increase in the electron temperature, resulting in an increase in the alpha heating power, and hence, a further increase in the total absorbed power. Thus, we introduced a simple control algorithm: a staged increase of the external heating power on the condition that the ratio of the edge electron density (electron density at ρ = 1) to the density limit reaches a pre-set value (0.7 was selected in this case). The external heating power needs to be shut off to move to the self-ignition condition in the final

phase of plasma start-up. We also adopted a simple algorithm, a staged decrease in the external heating power on the condition that the fusion power exceeds the target value. We also assumed discrete variations in the external heating power: minimum variation range and minimum variation interval of 1 MW and 1 s, respectively.

3.2. Confirmation of control method

Using the control algorithm described in the previous subsection, the ignition access of FFHR-d1 was examined. To save computational time, VMEC and GSRAKE calculations were performed at 2s and 10 s intervals in the simulation time, respectively.

The time evolution of the plasma and externally controlled parameters is summarised in Fig. 3. As shown in Fig. 3(a) and (e), the control algorithm of the external heating power works well and the fusion power can be smoothly changed. Although a slight overshoot of the fusion power is seen from Fig. 3(b), a steady-state, self-ignition operation around the target fusion power of ~3 GW was achieved. The magnitude of the overshoot depended on the target fusion power and the variation of the external heating power, hence it can be reduced by selecting optimum control parameters. In this case, the plasma start-up time was set to 300 s. Because characteristic time constant (e.g. energy confinement time) of the core plasma are of the order of 1 s or less, plasma start-up over a longer time period can be achieved using the same control method by changing the time over which the target line-averaged electron density is varied. The perturbation of the fusion power in the final (steady-state) phase is less than 2%, which is acceptable for the operation of the power generation system. As shown in Fig. 4, MHD equilibrium exists in this final state (after 400 s with a peak beta value ~6%). Because of the increase in volume inside the flux surfaces near the magnetic axis caused by the Shafranov shift, the fusion power at the same target value of the line-averaged electron density is slightly larger than the case without the equilibrium calculations. The pellet penetration depth also varies with the change in the shape of the flux surfaces around the edge. However, controllability of the fusion power was not affected by this level of the change and stable ignition access was achieved as long as the target value of the line-averaged electron density was properly set.

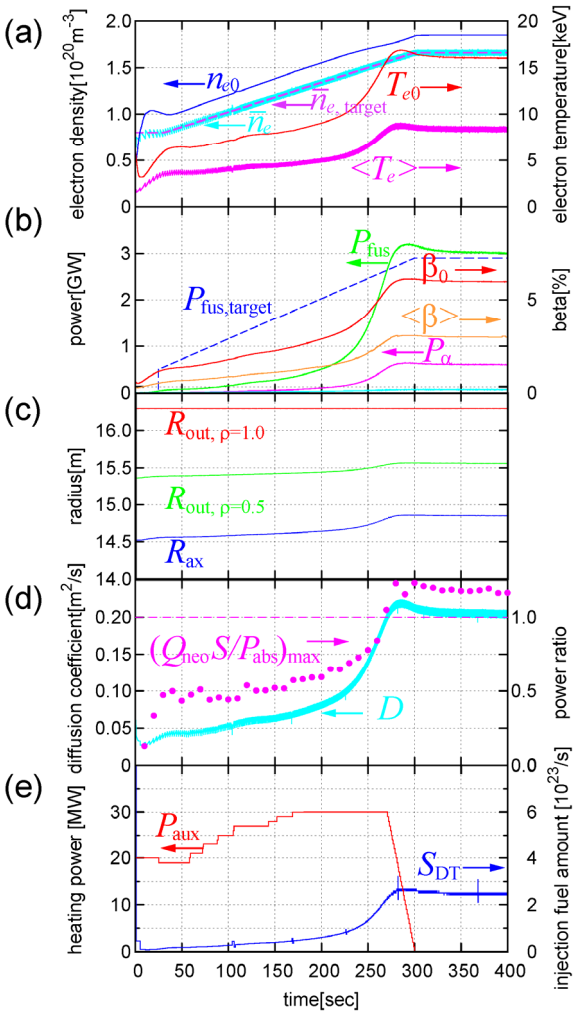

Figure 3. Time evolution of (a) the electron density and temperature, (b) the fusion power and beta value, (c) the magnetic axis position, (d) diffusion coefficient and the power balance (maximum value of the ratio of the neo-classical energy loss to the total absorbed power) and (e) the external heating power and the injected fuel for self-ignition operation.

However, the consistency between the power absorption with the neo-classical transport was not assured. Figure 5 shows the radial profiles of the neo-classical energy flux and the volume-integrated total absorbed power

at t = 400 s. There is an overbalance of approximately 60 MW at the radial position of ρ = 0.5. The closed circles in Fig. 3(d) show the maximum value along the radial profile of the ratio of neo-classical energy loss to the volume-integrated absorbed power for each time slice. It shows that the overbalance occurs during the final phase of the start-up with a large increase in the fusion power. Of course we should consider the contribution of anomalous transport to discuss the total power balance. But inward energy flux by anomalous transport is hardly expected and the neo-classical energy loss should be smaller than the total absorbed power for every flux surface. This large neo-classical energy loss is caused by the difference between the radial profile of the electron density and temperature at the steady state and that expected from the direct extrapolation of the reference experimental data (Fig. 6). As shown in Fig. 7, the pellet penetration depth is much shallower than that in the LHD experiments and becomes further shallower with increasing electron density and temperature. This shallow deposition causes a flat density profile, resulting in the lower density and higher temperature in the core region.

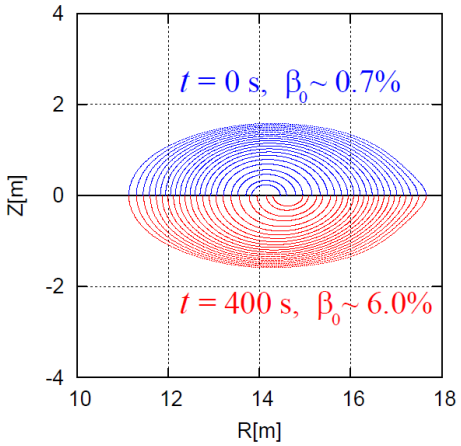

Figure 4. Flux surfaces at the initial (upper) and the final (lower) phase of the plasma start-up for self-ignition operation.

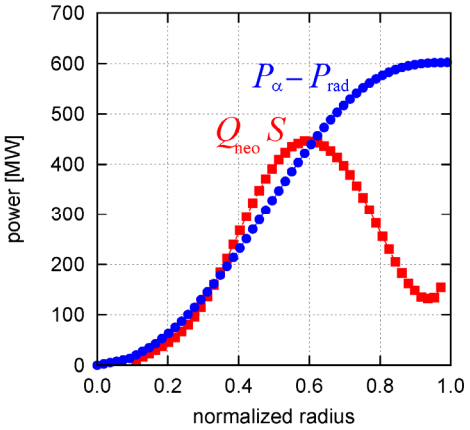

Figure 5. Radial profiles of the neo-classical energy flux and the volume-integrated total absorbed power for self-ignition operation.

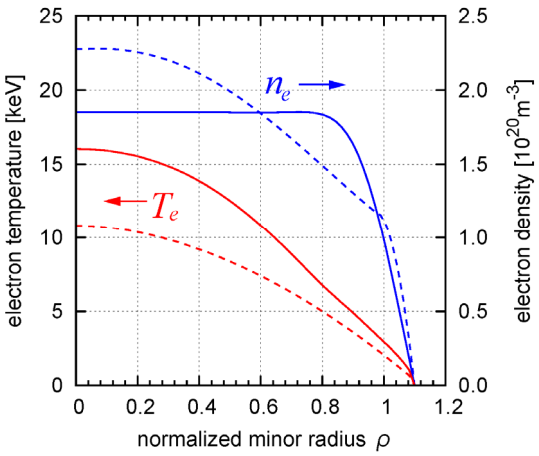

Figure 6. Comparison of the radial profiles of electron density and temperature at the steady state for self-ignition operation (solid lines) with that reconstructed from the normalised electron pressure using Eqs. (5) and (6) (broken lines).

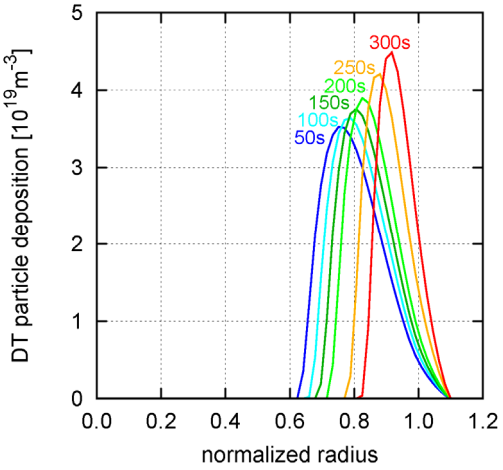

Figure 7. Time evolution of the radial profile of the pellet ablation for self-ignition operation. After reaching the steady-state (t > 300 s), the deposition profile also becomes constant.

4. Calculation result

4.1. Calculation of self-ignition operation

In general, neo-classical energy loss in low collisional regimes increases with increasing electron temperature and decreasing electron density. In actual situation, the increase of electron temperature is expected to be suppressed due to the degradation of the confinement caused by increasing neo-classical energy loss. We reflected this effect in our calculation by changing the electron temperature profile. In more detail, the gradient of the electron temperature over the region in which neo-classical energy loss exceeds the volume-integrated absorbed power was flattened until the maximum value in the radial profile of the ratio of the neo-classical energy loss to the volume-integrated absorbed power was equal to 0.95 (considering a 5% margin), as shown in Fig. 8. The temperature profile is recovered in the same manner if the ratio of the neo-classical energy loss to the volume-integrated absorbed power in the entire region is less than 0.95.

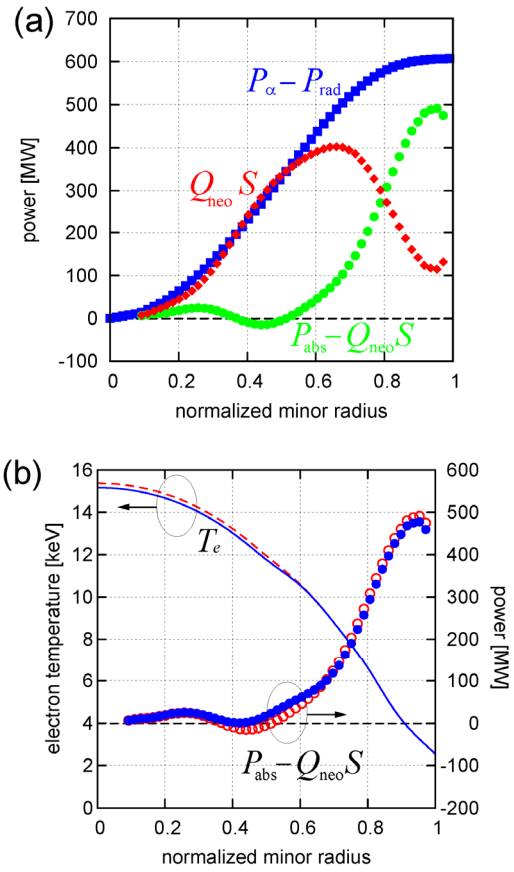

Figure 8. Electron temperature modification procedure. If neo-classical energy loss exceeds the volume-integrated total absorbed power (a), the temperature gradient of the region in which the power balance is not satisfied is flattened (compare broken line and solid line in (b)) until the power balance is satisfied (open circles to closed circles in (b)). Open circles in (b) correspond to the closed circles in (a).

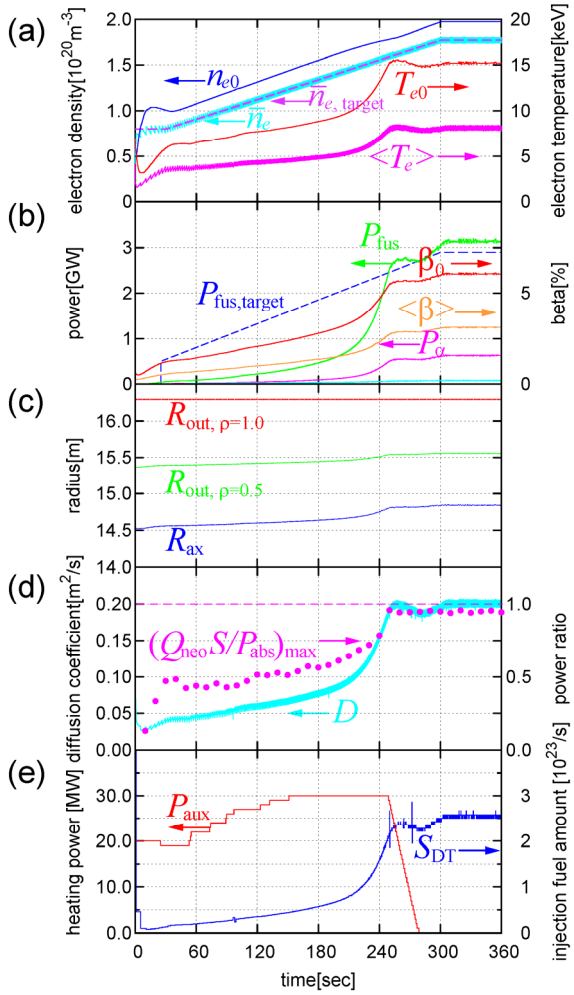

Figure 9. Time evolution of (a) the electron density and temperature, (b) the fusion power and beta value, (c) the magnetic axis position, (d) diffusion coefficient and the power balance (maximum value of the ratio of the neo-classical energy loss to the total absorbed power) and (e) the external heating power and the injected fuel for the calculations including the modification of the temperature profile.

Using this modified calculation procedure, the ignition access of FFHR-d1 was again examined. Figure 9 shows the time evolution of the plasma and externally-controlled parameters (same as those shown in Fig. 3). The radial profile of the pellet ablation is most identical to the previous case without the modification of the radial profile of the electron temperature. In this calculation, all control parameters except the target value of the line-averaged electron density were the same as those used in the calculations discussed in the previous subsection. In this case, the increase of the electron temperature stops earlier than the previous case and the final core electron temperature is lower (~15 keV). Because the increase of the electron temperature stops during the increasing phase of the electron density, the increase in the fusion power plateaued approximately t = 250 s and then slightly increased with increasing electron density up to 300 s where finally the steady-state, self-ignition condition was achieved with the fusion power at the target value (~3 GW). This indicates that the control method for the fuelling rate and the external heating also worked well for this case. Figure 10 compares the radial profile of the electron density and temperature at the final state for the calculation with and without the temperature modification. The electron temperature in the region of $\rho < 0.6$ is lower and the electron density in the entire region is higher in the case of the calculations with the modification of the temperature profile. Figure 11 shows the comparison of POPCON (Plasma OPeration CONtours) plot at the final state. In both cases, the final operation point locates the saddle point of the curve which represents the self-ignition condition (P_{aux} = 0), i.e. thermaly-stable region. But the location of the ignition condition curve moves to the upper-left of the plot (lower temperature, higher density) in the case of the calculation with the modification of the temperature profile.

In general, the operation density of helical reactors is higher than that of typical tokamak designs because there is no density limit caused by the plasma current. The operation temperature of helical reactors tends to be lower and the synchrotron radiation effect is not dominant. This fact is reflected in the smaller gradient of an upward-sloping section of the ignition condition curve compared with typical tokamak designs. As discussed in the previous study [8], this small gradient leads to very high sensitivity of the fusion power on the electron density. However, the results

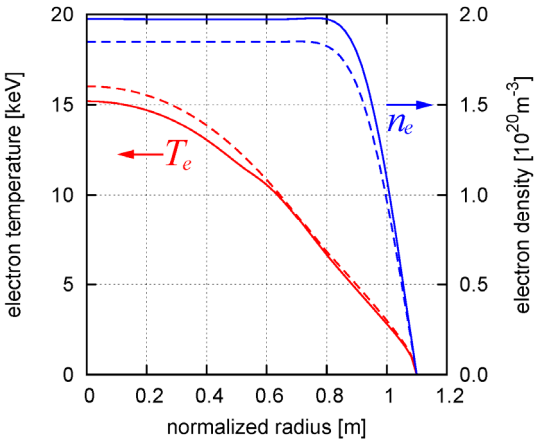

Figure 10. Comparison of the radial profile of electron density and temperature at the steady state with (solid lines) and without (broken lines) the modification of the radial profile of the electron temperature.

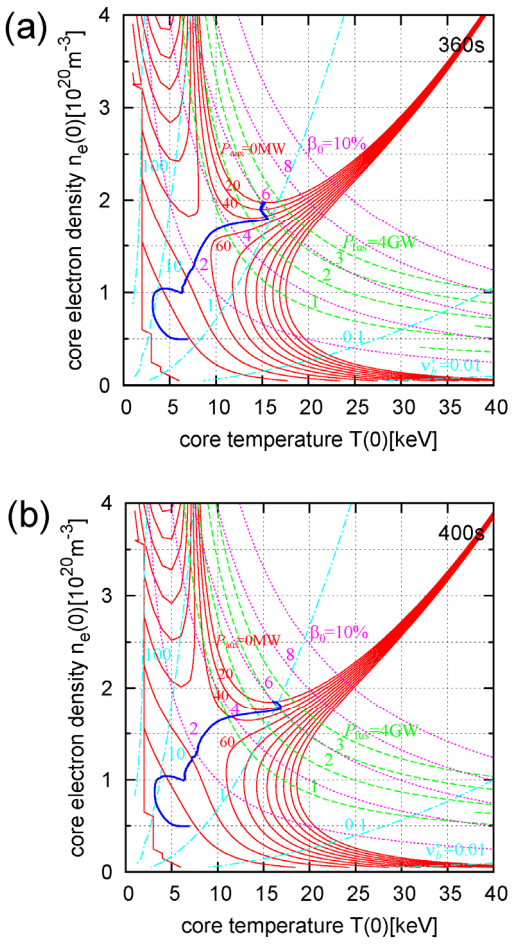

Figure 11. Comparison of the POPCON plot at the steady state (a) with and (b) without the modification of the radial profile of electron temperature.

of this study indicate that the operation point moves to the lower temperature and higher density region due to the degradation of the confinement caused by the increase in the neo-classical transport. It indicates that an abrupt increase in the fusion power with increasing electron temperature does not occur. In fact, overshoot of the fusion power was not observed when the temperature profile was modified, whereas it was difficult to completely suppress the overshoot of the fusion power in the previous calculation because the fusion power is inherently not suited to feedback control due to the large delay time and small time constant for the change. Although further detailed physics analyses are required to confirm these results, the suppression of the electron temperature and the fusion power due to an increase in the neo-classical energy loss may be an advantage considering the safety and controllability of the core plasma. The control method of the fuelling rate and the external heating power as proposed in this study indicates that only three measurements, the line-averaged electron density, the edge electron density and the fusion power (or neutron counting) are required. This stable and safe controllability of the core plasma with a small number of simple diagnostics is another advantage of the helical system.

4.2. Calculation of Sub-ignition operation

The operation control algorithm is also effective under sub-ignition operation conditions. As in the case of the self-ignition operation, steady-state with a sufficiently small perturbation of the fusion power can be achieved as long as the target line-averaged electron density is properly set. Figure 12 shows the time evolution of the plasma and external control parameters for a target electron density of 1.18×10^{20} m^{-3}. Figure 13 shows the time evolution of the radial profile of the pellet ablation. In the steady-state phase, a fusion power of ~600 MW with an external heating power of 30 MW, i.e. fusion gain Q ~ 20, can be achieved. In this case, the neo-classical energy loss is sufficiently small (~70%) compared with the volume-integrated absorbed power as shown in Fig. 12(d) and Fig. 14 because of the small Shafranov shift and low plasma temperature.

Of course the self-ignition operation is favourable to take full advantage of the characteristics of the net-current-free plasma of the helical system. Sub-ignition operation is important because it enables a flexible selection of the fusion power. Operation with a modest fusion power is particularly important in the early phase of the operation of the DEMO reactor to confirm the safety and integrity of the plant system. Sub-ignition operation also enables a wider selection of core plasma parameters, which leads to a flexible reactor design e.g. smaller reactor size, lower magnetic field strength.

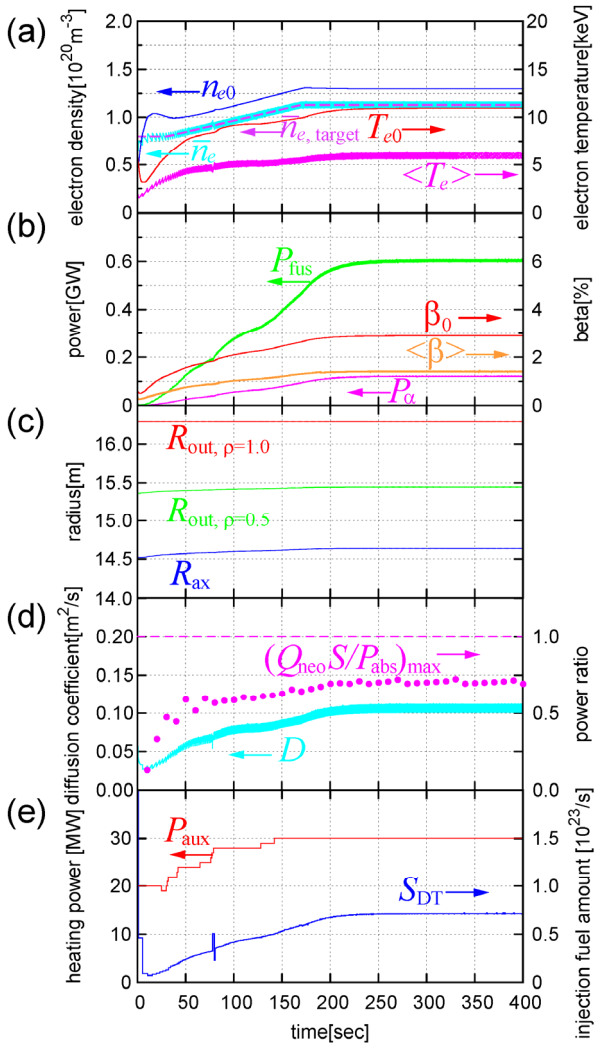

Figure 12. Time evolution of (a) the electron density and temperature, (b) the fusion power and beta value, (c) the magnetic axis position, (d) diffusion coefficient and the power balance (maximum value of the ratio of the neo-classical energy loss to the total absorbed power) and (e) external heating power and injected fuel for sub-ignition operation.

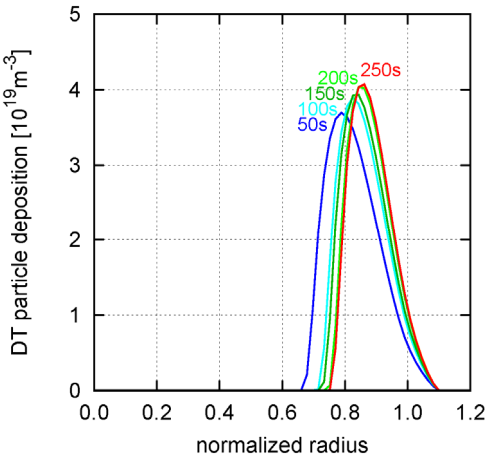

Figure 13. Time evolution of the radial profile of the pellet ablation for sub-ignition operation. After reaching the steady-state (t > 250 s), the deposition profile also becomes constant.

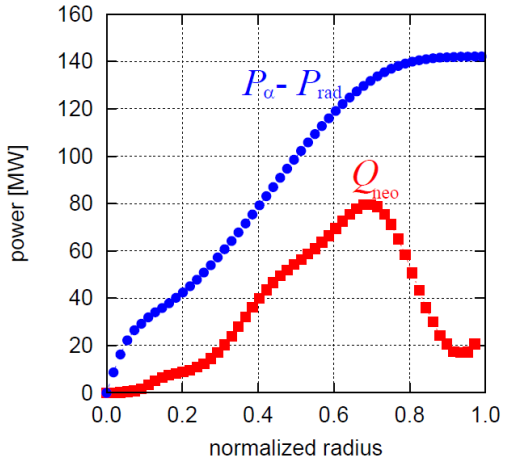

Figure 14. Radial profiles of the integrated total neo-classical energy flux and the volume-integrated total absorbed power for sub-ignition operation.

5. Summary

Plasma start-up scenarios for the LHD-type helical fusion reactor FFHR-d1 was examined using integrated 1D analysis code. An 'abductive' inference method based on the LHD experimental observations was adopted for fast estimation of the radial profiles of the reactor plasma. Consistency with MHD equilibrium and neo-classical transport was evaluated by coupling the 1D calculation model with the integrated transport analysis code TASK3D.

Stable and safe control of the fusion power was demonstrated with a small number of simple diagnostics (fuelling control based on line-averaged electron density and heating power control based on the edge electron density and the fusion power) for both self-ignition and sub-ignition conditions. This robust controllability comes from the characteristics of the net-current-free plasma. It is favourable to the design of peripheral and power plant equipment and can be another advantage of the helical system.

Although more precise physics analyses are required to confirm this start-up scenario (e.g. MHD stability, alpha particle confinement and energy transfer from electrons to ions), this study can provide a foundation for further analysis and engineering design of FFHR-d1 and other LHD-type helical reactors.

Acknowledgements

This study was supported by the budget NIFS10ULFF011 of National Institute for Fusion Science and MEXT/JSPS KAKENHI Grant Number 24760704. The authors also would like to acknowledge the members of the Fusion Engineering Research Project in NIFS for giving valuable comments and advice.

References

[1] Komori A. *et al* 2010 *Fusion Sci. Technol.* **58** 1
[2] Sagara A. *et al* 2012 *Fusion Eng. Des.* **87** 594
[3] Miyazawa J. *et al* 2011 *Fusion Eng. Des.* **86** 2879
[4] Goto T. *et al* 2012 *Plasma Fusion Res.* **7** 2405084
[5] Miyazawa J. *et al* 2014 *Nucl. Fusion* **54** 043010

[6] Mitarai O. *et al* 2007 *Nucl. Fusion* **47** 1411
[7] Sakamoto R. *et al* 2012 *Nucl. Fusion* **52** 083006
[8] Goto T. *et al* 2014 *Fusion Eng. Des.* **89** 2451
[9] Miyazawa J. *et al* 2014 *Nucl. Fusion* **54** 013014
[10] Parks P.B. *et al* 1978 *Phys. Fluids* **21** 1735
[11] Yokoyama M. *et al* 2013 *Plasma Fusion Res.* **8** 2403016
[12] Hirshman S.P. *et al* 1983 *Phys. Fluids* **26** 3553
[13] Beidler C.D. *et al* 1995 *Plasma Phys. Control. Fusion* **37** 463
[14] Watanabe K.Y. *et al* 2004 *Fusion Sci. Technol.* **46** 24
[15] Watanabe K.Y. *et al* 2010 *Fusion Sci. Technol.* **58** 160
[16] Suzuki Y. *et al* 2006 *Nucl. Fusion* **46** L19
[17] Miyazawa J. *et al* 2008 *Nucl. Fusion* **48** 015003